Electronic Supplementary Information

A Structural Parameter to Link Molecular Geometry to Macroscopic Orientation in Discotic Liquid Crystals: Study of Metalloporphyrin Tapes

Yoshiyuki Kobayashi,[a] Atsuya Muranaka,[b] Kenichi Kato,[c] Akinori Saeki,[d] Takayuki Tanaka,[e] Masanobu Uchiyama,[b] Atsuhiro Osuka,[e] Takuzo Aida*[a] and Tsuneaki Sakurai,*[af]

[a] *Department of Chemistry and Biotechnology, School of Engineering, The University of Tokyo, 7-3-1 Hongo, Bunkyo-ku, Tokyo, 113-8656, Japan.*

[b] *Elements Chemistry Laboratory, RIKEN, and Advanced Elements Chemistry Research Team, RIKEN, Center for Sustainable Resource Science (CSRS), Wako, Saitama 351-0198, Japan*

[c] *RIKEN SPring-8 Center, 1-1-1 Kouto, Sayo-cho, Sayo-gun, Hyogo, 679-5148, Japan.*

[d] *Department of Applied Chemistry, Graduate School of Engineering, Osaka University, 2-1 Yamadaoka, Suita, Osaka, 565-0871, Japan.*

[e] *Department of Chemistry, Graduate School of Science, Kyoto University, Sakyo-ku, Kyoto 606-8502, Japan.*

[f] *Faculty of Molecular Chemistry and Engineering, Kyoto Institute of Technology, Matsugasaki, Sakyo-ku, Kyoto 606-8585, Japan.*

*Correspondence and requests for materials should be addressed to Tsuneaki Sakurai (sakurai@kit.ac.jp) and Takuzo Aida (aida@macro.t.u-tokyo.ac.jp).

Table of Contents

1. General

Unless otherwise noted, all commercial reagents were used as received from Tokyo Kasei Co., Aldrich, and Wako. Anhydrous solvents for reactions were purchased from Kanto Chemicals. Recycling preparative high-performance liquid chromatography (HPLC) was performed at room temperature using a 20 mm × 250 mm silica gel column (JAIGEL SIL SH043-10) on a Japan Analytical Industry LC-918 HPLC system, equipped with a variable-wavelength UV-Vis detector. Thin layer chromatography (TLC) was performed by silica gel 60 F_{254}. Preparative separations were performed by silica gel chromatography (Wako gel C-400) or size exclusion gel permeation chromatography (Bio-Rad Bio-Beads S-X1, packed with THF in a 5 x 100 cm gravity column). ^{1}H NMR spectra were recorded in $CDCl_3$ or THF-d_8 on a JEOL GSX-270 spectrometer operating at 270 MHz, and a JEOL NM-Excalibur 500 spectrometer operating at 500 MHz, where chemical shifts were determined with respect to $CHCl_3$ or THF as an internal reference. Matrix-assisted laser desorption/ionization time-of-flight (MALDI-TOF) mass spectrometry was performed on a Bruker Daltonics ultrafleXtreme spectrometer using reflector positive mode and DCTB as a matrix. HPLC analysis was performed by eluting a THF solution of $\mathbf{1}_{\mathbf{Zn}}$ with Shimadzu HPLC Prominence equipped with a SUMICHIRAL OA-3100 column (φ = 4.6 mm) using THF/hexane (v/v = 5/95) as an eluent. Electronic absorption spectra were recorded on a JASCO model U-best V-570 spectrometer. DSC measurements were performed on a Mettler model DSC 1 differential scanning calorimeter. Cooling and heating profiles were recorded and analyzed with a Mettler model STARe system. Polarized optical microscopy was performed on an Olympus model BX 51 optical polarizing microscope equipped with a Mettler–Toledo model FP–82HT hot stage. Samples were introduced into an ITO-coated glass cell, where two glass substrates were spaced by 5 μm-diameter silica beads. X-ray diffraction experiments were carried out using a synchrotron radiation X-ray beam with a wavelength of 1.08 Å on BL44B2 at the Super Photon Ring (SPring-8, Hyogo, Japan). A large Debye-Scherrer camera was used in conjunction with an imaging plate as a detector, and all diffraction patterns were obtained with a 0.01º step in 2θ. During the measurements, all samples, put into a 0.5-mm thick glass capillary, were rotated to obtain homogeneous diffraction patterns. The exposure time to the X-ray beam was 2 min. Flash-photolysis time-resolved microwave conductivity (FP-TRMC) measurements were

carried out at 20 °C in air, where the resonant frequency and microwave power were properly adjusted at 9.1 GHz and 3 mW, respectively. Charge carriers were photochemically generated using a third harmonic generation (λ = 355 nm) of a Spectra Physics model GCR-130 Nd:YAG laser with a pulse duration of 5–8 ns. The photon density was 1.2 x 10^{16} photons cm^{-2}. The TRMC signal, picked up by a diode (rise time < 1 ns), was monitored by a Tektronics model TDS3052B digital oscilloscope. The observed conductivities were normalized, given by a photocarrier generation yield (ϕ) multiplied by sum of the charge carrier mobilities ($\Sigma\mu$), according to the equation, $\phi\Sigma\mu = (1/eAI_0F_{light})(\Delta P_r/P_r)$, where, e, A, I_0, F_{light}, P_r, and ΔP_r are the unit charge of a single electron, a sensitivity factor (S^{-1} cm), an incident photon density of the excitation laser (photon cm^{-2}), a correction (or filling) factor (cm^{-1}), and a reflected microwave power and its change, respectively. All calculations were performed at the DFT level, by means of the hybrid Becke3LYP (B3LYP) (*S1–S3*) functional as implemented in Gaussian 09 (*S4*). The 6-31G(d) basis set was used for C, H, and N atoms, while LanL2DZ basis set was used for metal atoms. In order to investigate the planarity of *meso*-alkyl fused porphyrin dimers, geometry optimizations of *meso*-methyl fused dimers were carried out by considering two nonplanar initial geometries. Two metal ions were located on the same side of the macrocycle for one initial structure, while the position of two metal ions was set to be oriented in opposing directions for the other geometry. For all converged structures, frequency calculations were carried out at the same level to discern between minima and transition states.

2. Synthesis

2.1. Synthesis of Compound 2

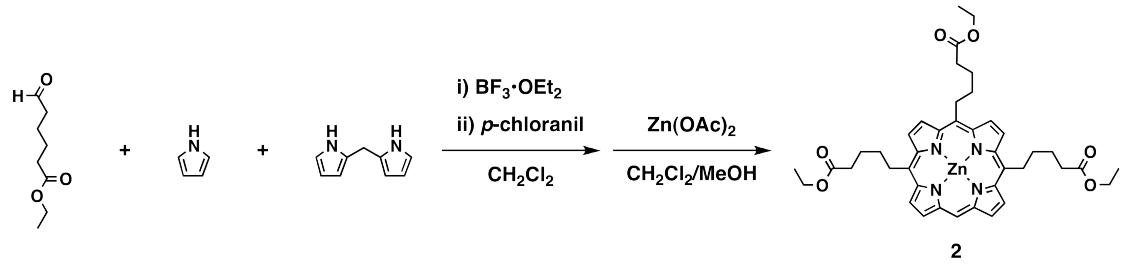

2

2: To a CH_2Cl_2 solution (750 mL) of a mixture of ethyl 6-oxohexanoate (*S5*) (1.92 g, 12.1 mmol), pyrrole (0.542 g, 8.08 mmol) and dipyrromethane (0.591 g, 4.04 mmol) was added $BF_3{\cdot}OEt_2$ (0.075 mL), and the mixture was stirred for 24 h at 20 °C under argon. To the reaction mixture was added 2,3,5,6-tetrachloro-1,4-benzoquinone (*p*-chloranil) (2.56 g, 10.4 mmol), and the mixture was stirred for 2 h at 20 °C and then quenched with triethylamine. The solution containing the reaction mixture was concentrated to a volume of 100 mL and then chromatographed on alumina with CH_2Cl_2 followed by silica gel with CH_2Cl_2 as eluent, where the reddish purple fraction was collected and evaporated to dryness. The residue was subjected to SEC (Bio–Rad Bio–Beads S–XI) with THF as an eluent, where the second fraction (reddish purple color) was collected and evaporated. To a CH_2Cl_2 solution (100 mL) of the residue was added a saturated MeOH solution (10 mL) of $Zn(OAc)_2$, and the mixture was stirred for 3 h at 20 ºC. The reaction mixture was washed with water, dried over Na_2SO_4, and evaporated to dryness. The residue was chromatographed on silica gel with CH_2Cl_2/EtOAc (10/1) as an eluent, where the first fraction was collected and evaporated to allow isolation of **2** as red solid (162 mg, 0.214 mmol, 5%). ^{1}H NMR ($CDCl_3$) δ 8.95 (s, 1H, meso-H), 8.68–8.60 (m, 6H, pyrrole-β-H), 8.52 (d, 2H, pyrrole-β-H), 4.20–4.13 (m, 6H, C*H*$_2$CH$_2$CH$_2$CH$_2$COOCH$_2$CH$_3$), 4.11–4.03 (m, 6H, CH$_2$CH$_2$CH$_2$CH$_2$COOC*H*$_2$CH$_3$), 2.40–2.32 (m, 6H, CH$_2$C*H*$_2$CH$_2$CH$_2$COOCH$_2$CH$_3$), 2.24–2.11 (m, 6H, CH$_2$CH$_2$C*H*$_2$CH$_2$COOCH$_2$CH$_3$), 2.03–1.93 (m, 6H, CH$_2$CH$_2$CH$_2$C*H*$_2$COOCH$_2$CH$_3$), 1.23–1.17 (m, 9H, CH$_2$CH$_2$CH$_2$CH$_2$COOCH$_2$C*H*$_3$); MALDI-TOF-MS *m/z* calcd. for $C_{41}H_{48}N_4O_6Zn$ (M^+) 758.24, found 756.47.

2.2. Synthesis of Compound 3

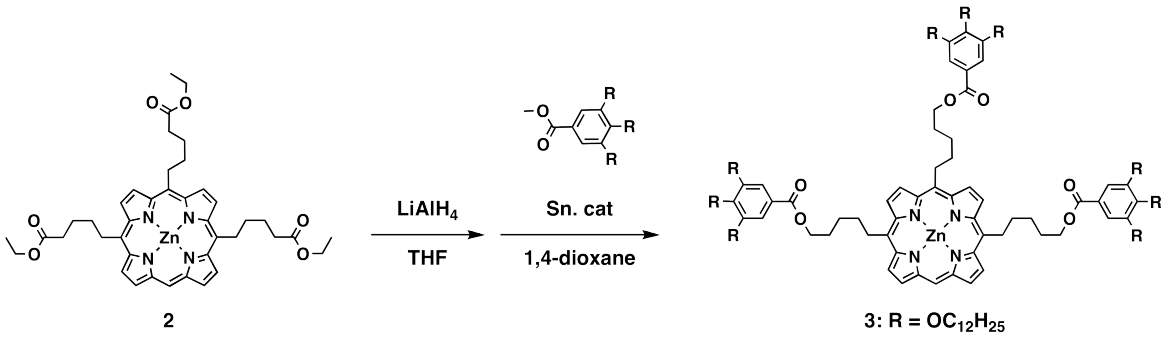

3: To a THF solution (20 mL) of **2** (0.220 g, 0.291 mmol) was dropwise added a THF solution (20 mL) of $LiAlH_4$ (36.4 mg, 0.960 mmol) at 0 ºC, and the mixture was stirred for 2 h at 20 ºC. After the dropwise addition of water/THF (1/1 v/v) solution (2 mL) at 0 ºC, the reaction mixture was filtered off from insoluble fraction and evaporated. The residue was dissolved in diethyl ether, washed with water, dried over Na_2SO_4, and evaporated to dryness. To a 1,4-dioxane (20 mL) solution of the residue were successively added 3,4,5-tris-dodecyloxy-methyl benzoate (*S6*) (2.38 g, 3.45 mmol) and distannoxane catalyst (*S7*) (37.0 mg, 34.5 μmol), and the mixture was refluxed for 60 h under argon. The solution containing the reaction mixture was concentrated and then subjected to SEC with THF as an eluent, where the first reddish fraction was collected and evaporated. The residue was chromatographed on silica gel with CH_2Cl_2 as an eluent, where the first fraction was collected and evaporated to allow isolation of **3** as a red solid (450 mg, 0.173 mmol, 59%). ^{1}H NMR ($CDCl_3$) δ 9.81 (s, 1H, meso-H), 9.50–9.47 (m, 6H, pyrrole-β-H), 9.21 (d, 2H, pyrrole-β-H), 8.91 (s, 6H, Ar-H), 5.00–4.92 (m, 6H, C*H*$_2$CH$_2$CH$_2$CH$_2$CH$_2$OCOAr), 4.39–4.37 (m, 6H, CH$_2$CH$_2$CH$_2$CH$_2$C*H*$_2$OCOAr), 4.01–3.95 (m, 18H, OC*H*$_2$(CH$_2$)$_{10}$CH$_3$), 3.77–3.73 (m, 6H, CH$_2$C*H*$_2$CH$_2$CH$_2$CH$_2$OCOAr), 3.71–3.66 (m, 6H, CH$_2$CH$_2$CH$_2$C*H*$_2$CH$_2$OCOAr), 2.63–2.57 (m, 6H, CH$_2$CH$_2$C*H*$_2$CH$_2$CH$_2$OCOAr), 1.99–1.22 (m, 180H, OCH$_2$(C*H*$_2$)$_{10}$CH$_3$), 0.92–0.83 (m, 27H, OCH$_2$(CH$_2$)$_{10}$C*H*$_3$); MALDI-TOF-MS *m/z* calcd. for $C_{164}H_{270}N_4O_{15}Zn$ (M^+) 2603.36, found 2601.56.

2.3. Synthesis of Compound $\mathbf{1}_{Zn}$

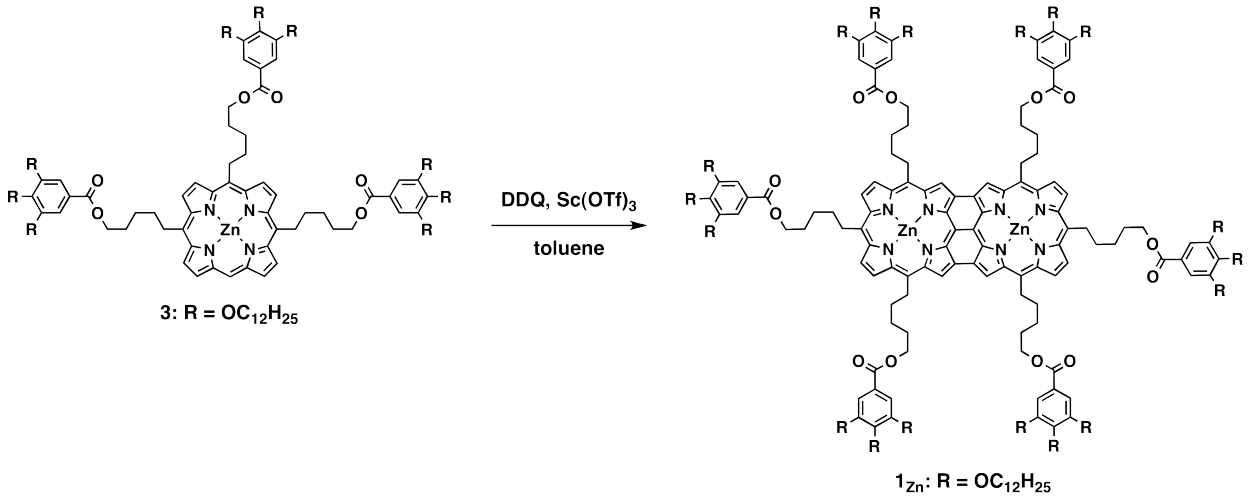

$\mathbf{1}_{Zn}$: A solution of **3** (321 mg, 0.123 mmol) in dry toluene (130 mL) was degassed by argon and warmed up to 50 ºC. Then 2,3-dichloro-5,6-dicyano-1,4-benzoquinone (DDQ) (83.7 mg, 0369 mmol) and $Sc(OTf)_3$ (212 mg, 0.431 mmol) were added and the resulting mixture was stirred for 1 h at 50 °C under Ar. The reaction mixture was diluted with THF and chromatographed on alumina with THF as an eluent, where the first fraction was collected and evaporated to dryness. The residue was subjected to recycling preparative HPLC (JAIGEL-SIL) with hexane/THF (9/1) as an eluent at a flow rate of 9.9 mL min^{-1}, where the first fraction was collected and evaporated. The residue was subjected to reprecipitation repeatedly from dichloromethane/acetone to allow isolation of **$\mathbf{1}_{Zn}$** as a red solid (138 mg, 53 μmol, 43%). ^{1}H NMR (THF-d_8) δ 8.37–8.32 (m, 8H, pyrrole-β-H), 7.98 (s, 4H, pyrrole-β-H), 7.30 (s, 12H, Ar-H), 4.37–4.32 (m, 12H, CH_2(CH_2)$_3$$CH_2$OCOAr), 4.02–3.95 (m, 36H, OCH_2(CH_2)$_{10}$$CH_3$), 3.93–3.90 (m, 12H, CH_2(CH_2)$_3$CH_2OCOAr), 2.26–1.27 (m, 396H, CH_2(CH_2)$_3$$CH_2$OCOAr and OCH_2(CH_2)$_{10}$$CH_3$), 0.90–0.85 (m, 54H, OCH_2(CH_2)$_{10}$CH_3); MALDI-TOF-MS *m/z* calcd. for $C_{328}H_{534}N_8O_{30}Zn_2$ (M^+) 5200.67, found 5198.83.

2.4. Synthesis of Compound $\mathbf{1}_{2H}$

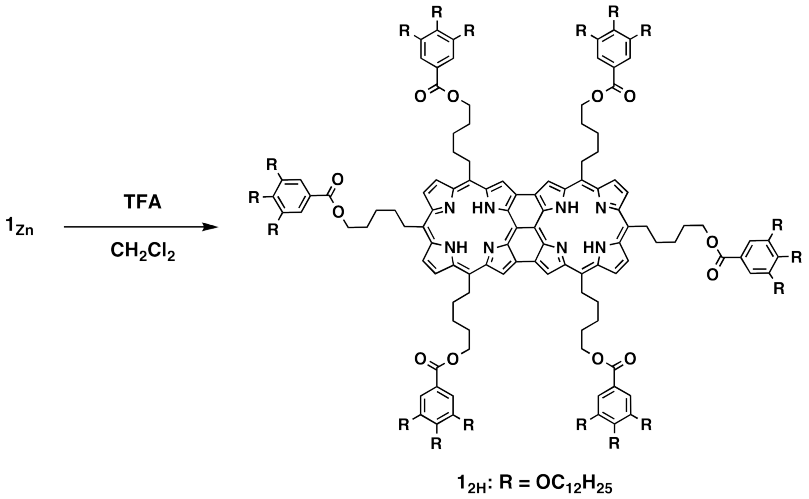

$\mathbf{1}_{2H}$: To a CH_2Cl_2 solution (100 mL) of **$\mathbf{1}_{Zn}$** (140 mg, 26.9 μmol) was added trifluoroacetic acid (TFA) (4.60 g, 40.3 mmol), and the mixture was stirred for 6 h at 20 °C. The reaction mixture was washed with saturated aqueous $NaHCO_3$, dried over Na_2SO_4, filtered through silica gel, and evaporated to dryness. The residue was subjected to recycling preparative HPLC (JAIGEL-SIL) with hexane/THF (9/1) as an eluent at a flow rate of 9.9 mL min^{-1}, where the first fraction was collected and evaporated. The residue was subjected to reprecipitation repeatedly from dichloromethane/acetone to allow isolation of **$\mathbf{1}_{2H}$** as a red solid (121 mg, 24 μmol, 89%). ^{1}H NMR (THF-d_8) δ 8.34–8.27 (m, 8H, pyrrole-β-H), 7.93 (s, 4H, pyrrole-β-H), 7.25 (s, 12H, Ar-H), 4.39–4.34 (m, 12H, CH_2(CH_2)$_3$$CH_2$OCOAr), 4.01–3.80 (m, 48H, OCH_2(CH_2)$_{10}$$CH_3$ and CH_2(CH_2)$_3$CH_2OCOAr), 2.26–1.24 (m, 400H, NH, CH_2(CH_2)$_3$$CH_2$OCOAr, and OCH_2(CH_2)$_{10}$$CH_3$), 0.89–0.83 (m, 54H, OCH_2(CH_2)$_{10}$CH_3); MALDI-TOF-MS *m/z* calcd. for $C_{328}H_{538}N_8O_{30}$ ([M + H]$^+$) 5073.94, found 5074.13.

2.5. Synthesis of Compounds $\mathbf{1}_{Pd}$ and $\mathbf{1}_{Ni}$

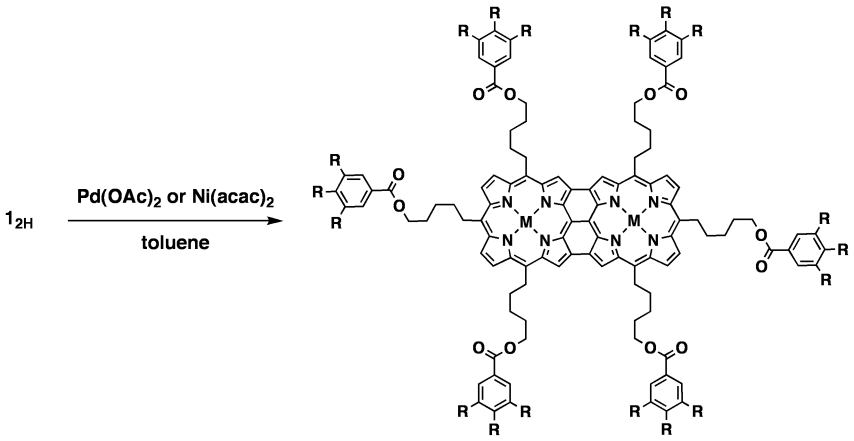

$\mathbf{1}_{Pd}$: To a toluene solution (50 mL) of **$\mathbf{1}_{2H}$** (71 mg, 14.0 μmol) was added $Pd(OAc)_2$ (100 mg, 0.44 mmol), and the mixture was refluxed for 6 h under argon. The reaction mixture was washed with water, dried over Na_2SO_4, filtered through silica gel, and evaporated to dryness. The residue was subjected to recycling preparative HPLC (JAIGEL-SIL) with hexane/THF (9/1) as an eluent at a flow rate of 9.9 mL min^{-1}, where the first fraction was collected and evaporated. The residue was subjected to reprecipitation repeatedly from dichloromethane/acetone to allow isolation of **$\mathbf{1}_{Pd}$** as a red solid (53 mg, 10 μmol, 71%). MALDI-TOF-MS *m/z* calcd. for $C_{328}H_{534}N_8O_{30}Pd_2$ (M^+) 5282.75, found 5281.16.

$\mathbf{1}_{Ni}$: To a toluene solution (50 mL) of **$\mathbf{1}_{2H}$** (78 mg, 15.3 μmol) was added $Ni(acac)_2$ (100 mg, 0.39 mmol), and the mixture was refluxed for 18 h under argon. The reaction mixture was washed with water, dried over Na_2SO_4, filtered through silica gel, and evaporated to dryness. The residue was subjected to recycling preparative HPLC (JAIGEL-SIL) with hexane/THF (9/1) as an eluent at a flow rate of 9.9 mL min^{-1}, where the first fraction was collected and evaporated. The residue was subjected to reprecipitation repeatedly from dichloromethane/acetone to allow isolation of **$\mathbf{1}_{Ni}$** as a red solid (40 mg, 7.7 μmol, 50%). MALDI-TOF-MS *m/z* calcd. for $C_{328}H_{534}N_8O_{30}Ni_2$ (M^+) 5187.29, found 5186.54.

2.6. Synthesis of Compound $\mathbf{1_{Cu}}$

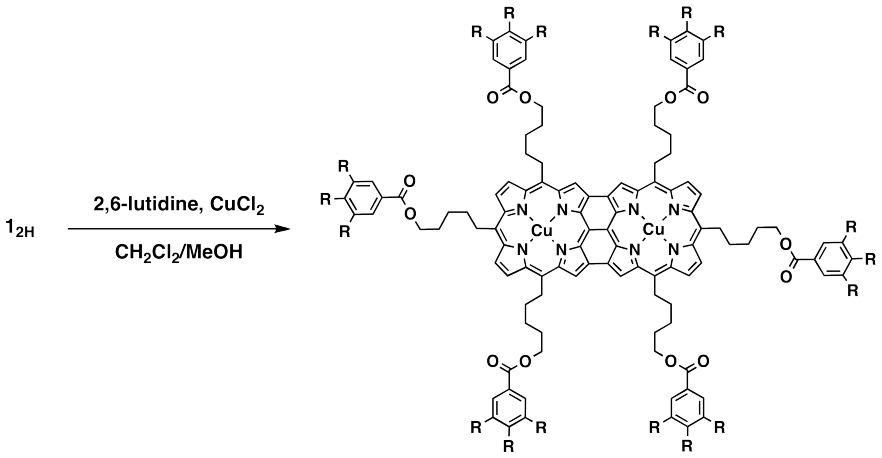

$\mathbf{1_{Cu}}$: R = $OC_{12}H_{25}$

$\mathbf{1_{Cu}}$: To a CH_2Cl_2/MeOH (10/1 v/v) solution (55 mL) of **$\mathbf{1_{2H}}$** (60 mg, 11.8 μmol) were successively added 2,6-lutidine (0.925 g, 8.63 mmol) and $CuCl_2$ (300 mg, 2.23 mmol), and the mixture was stirred for 18 h at 20 °C under argon. The reaction mixture was washed with water, dried over Na_2SO_4, filtered through silica gel, and evaporated to dryness. The residue was subjected to recycling preparative HPLC (JAIGEL-SIL) with hexane/THF (9/1) as an eluent at a flow rate of 9.9 mL min^{-1}, where the first fraction was collected and evaporated. The residue was subjected to reprecipitation repeatedly from dichloromethane/acetone to allow isolation of **$\mathbf{1_{Cu}}$** as a red solid (24 mg, 4.7 μmol, 39%). MALDI-TOF-MS *m/z* calcd. for $C_{328}H_{534}N_8O_{30}Cu_2$ (M^+) 5196.66, found 5196.11.

3. Supporting Figures

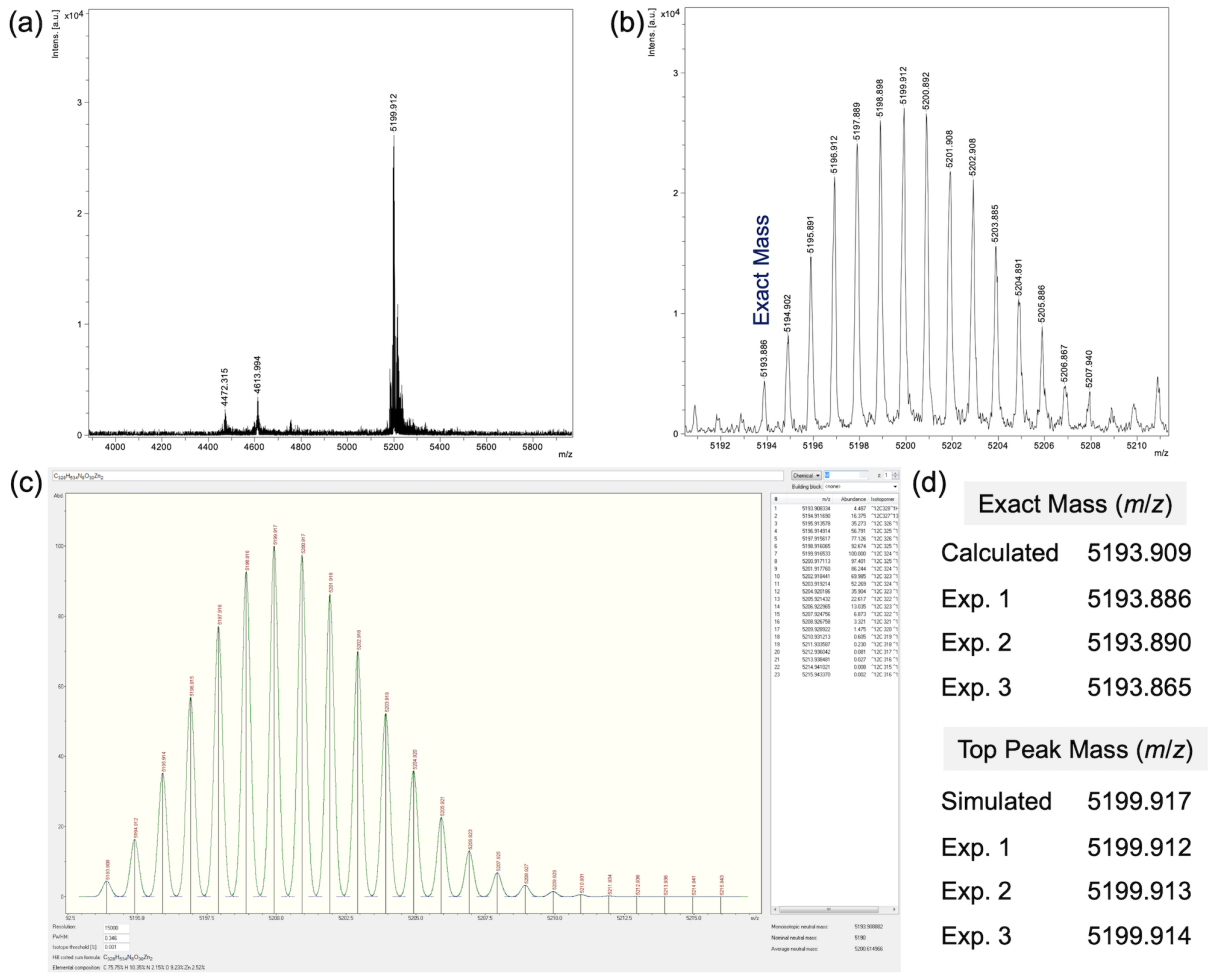

Figure S1. (a) Wide-range and (b) magnified MALDI-TOF MS spectra of $\mathbf{1}_{\mathbf{Zn}}$. (c) Simulated MS spectra of $\mathbf{1}_{\mathbf{Zn}}$. (d) Summary of calculated exact mass, simulated top peak mass, and experimentally observed exact and top peak mass values (three runs). The peaks at *m*/*z* of 4400–4800 may be due to the fragmentation of the compound.

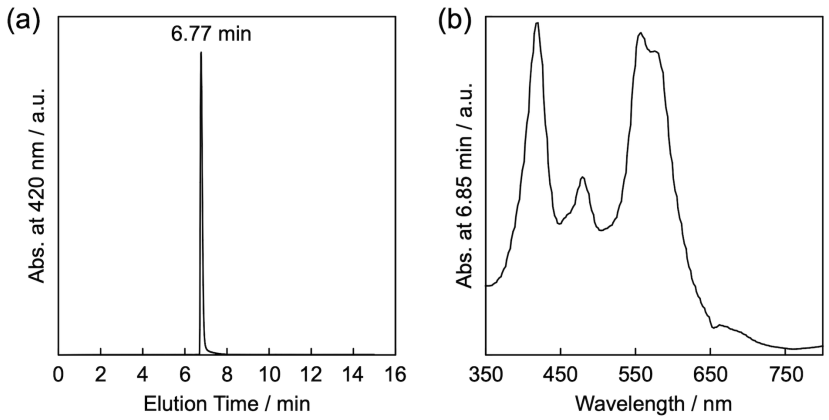

Figure S2. (a) Analytical HPLC chart of $\mathbf{1}_{\mathbf{Zn}}$. (b) Absorption spectra at 6.85 min in (a).

(a)

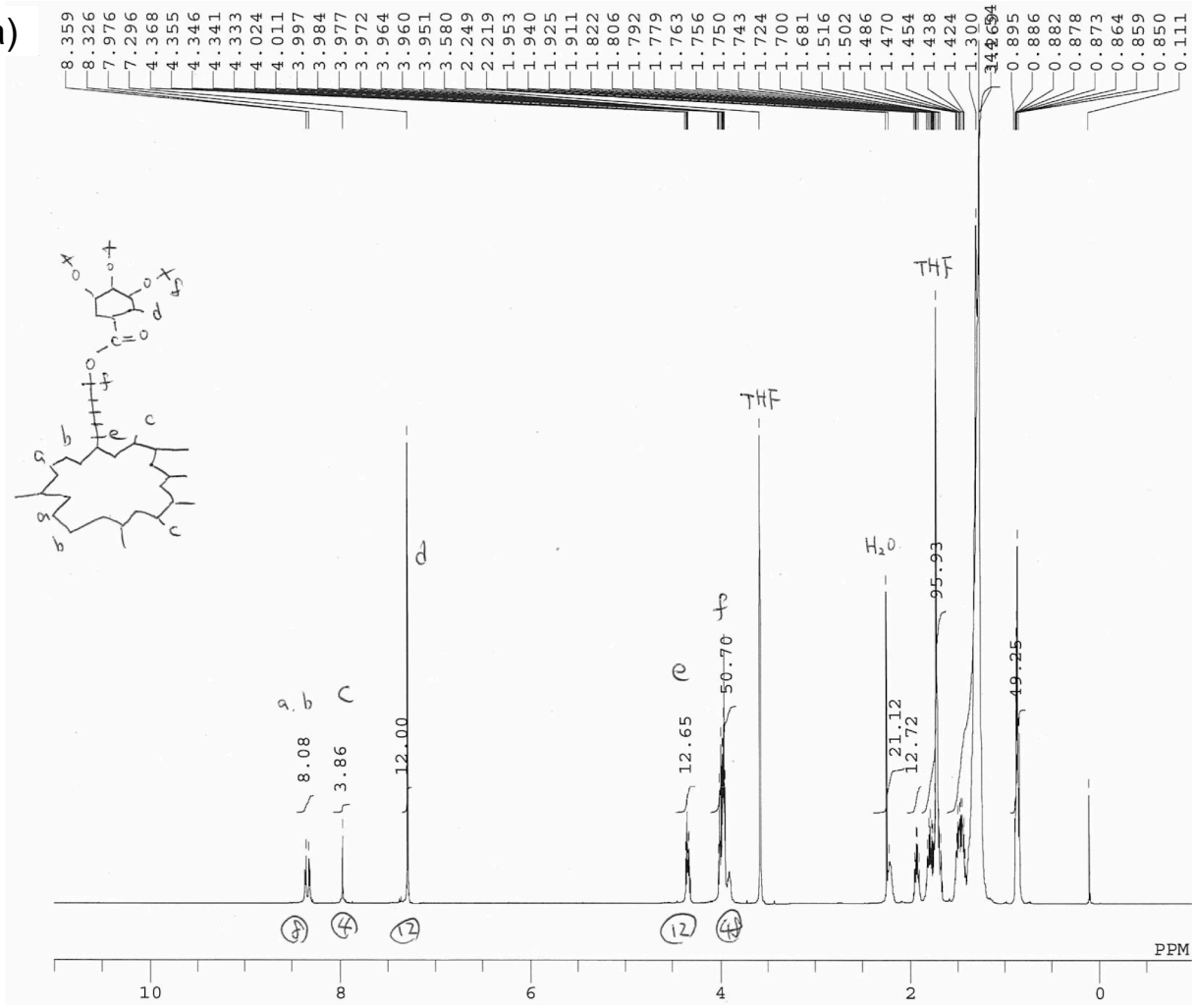
8.359
8.326
7.976
7.296
4.368
4.355
4.346
4.341
4.333
4.024
4.011
3.997
3.984
3.977
3.972
3.964
3.960
3.951
3.580
2.249
2.219
1.953
1.940
1.925
1.911
1.822
1.806
1.792
1.779
1.763
1.756
1.750
1.743
1.724
1.700
1.681
1.516
1.502
1.486
1.470
1.454
1.438
1.424
1.300
0.895
0.886
0.882
0.878
0.873
0.864
0.859
0.850
0.111
THF
THF
H₂O
a, b
8.08
c
3.86
d
12.00
e
12.65
f
50.70
21.12
12.72
95.93
49.25
PPM
10
8
6
4
2
0

(b)

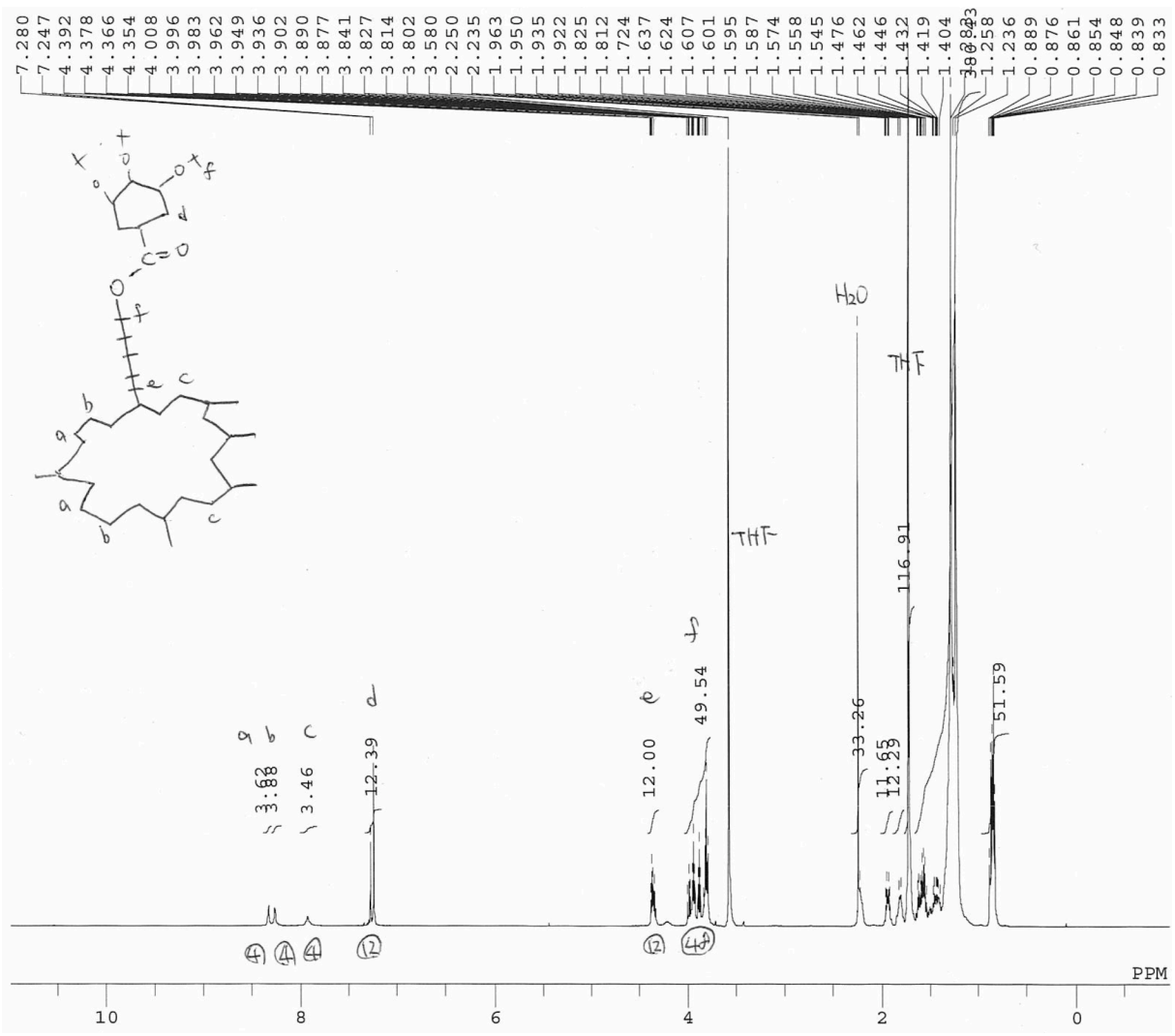

Figure S3. ^{1}H NMR spectra of (a) $\mathbf{1}_{\mathbf{Zn}}$ and (b) $\mathbf{1}_{\mathbf{2H}}$ in THF-d_8 at 60 ºC. A broad peak at ~4.2 ppm represents inner porphyrin NH protons of triply-linked dimeric porphyrins.

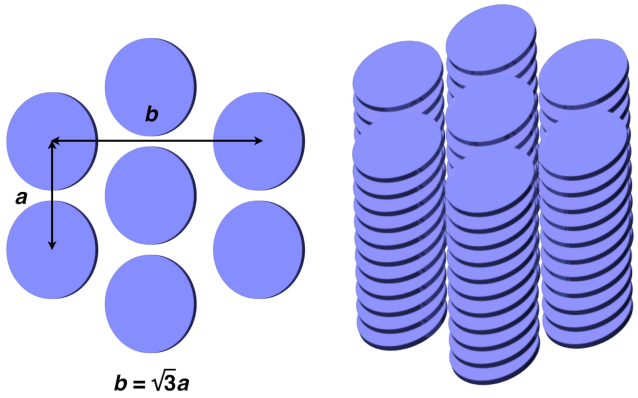

Figure S4. Schematic illustrations of packing structures of $\mathbf{1_M}$ in its LC mesophase. Discotic columns are composed of π-stacked fused porphyrin cores with a tilted fashion. The mesophase is pseudo-hexagonal when $b = \sqrt{3}a$.

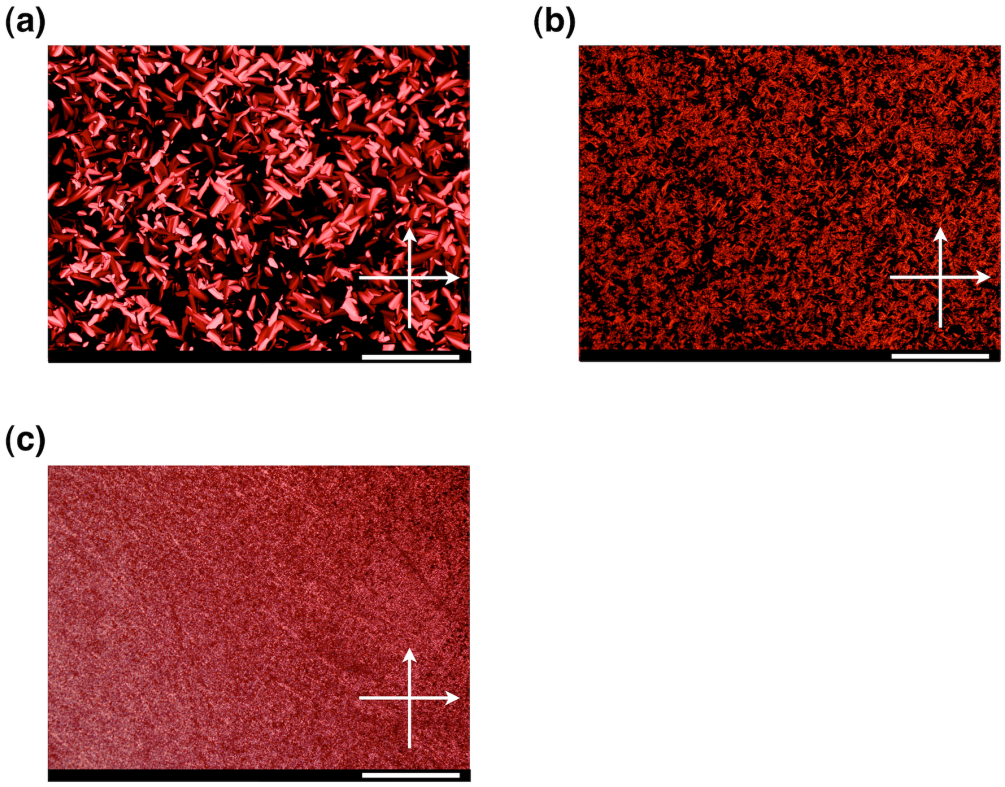

Figure S5. Crossed polarized micrographs of (a) $\mathbf{1_{Ni}}$ at 75 ºC, (b) $\mathbf{1_{2H}}$ at 86 ºC, and (c) $\mathbf{1_{Cu}}$ at 100 ºC. The samples were cooled at 20 ºC min^{-1} from the isotropic phase. The scale bars indicate 100 μm.

Additional Note: The presence/absence of textures were not largely changed at cooling rate of 1 ºC/min (Fig. 4.) and 0.1 ºC/min. It indicates that the bulk nucleation rate is not negligible compared with the nucleation from the surface for these compounds for $\mathbf{1_{Pd}}$ and $\mathbf{1_{Zn}}$.

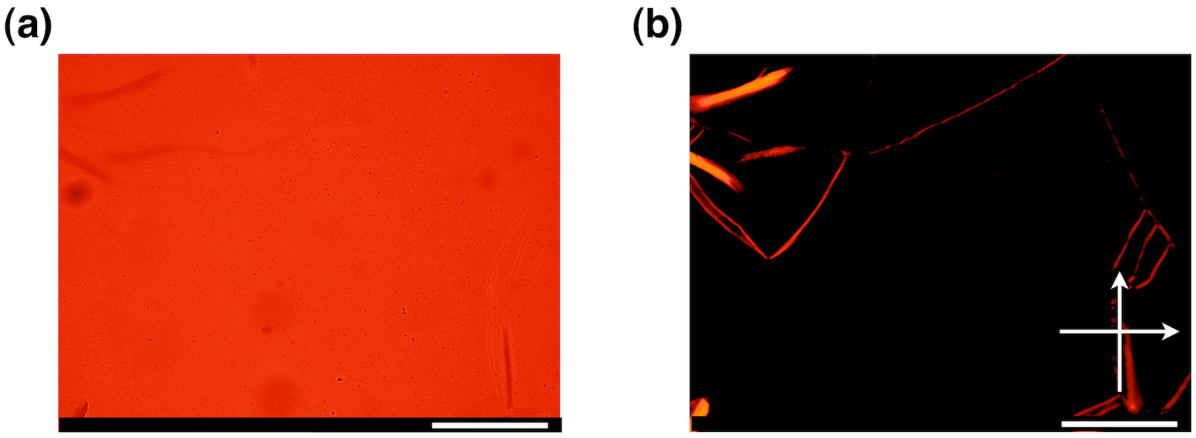

Figure S6. (a) Optical and (b) crossed polarized micrograph of $\mathbf{1}_{Ni}$ at 25 ºC. The sample was cooled at 1 ºC min^{-1} from isotropic phase. The scale bars indicate 100 μm. The bright lines and area in (b) indicate the domain boundaries where parallel orientation of columns takes place.

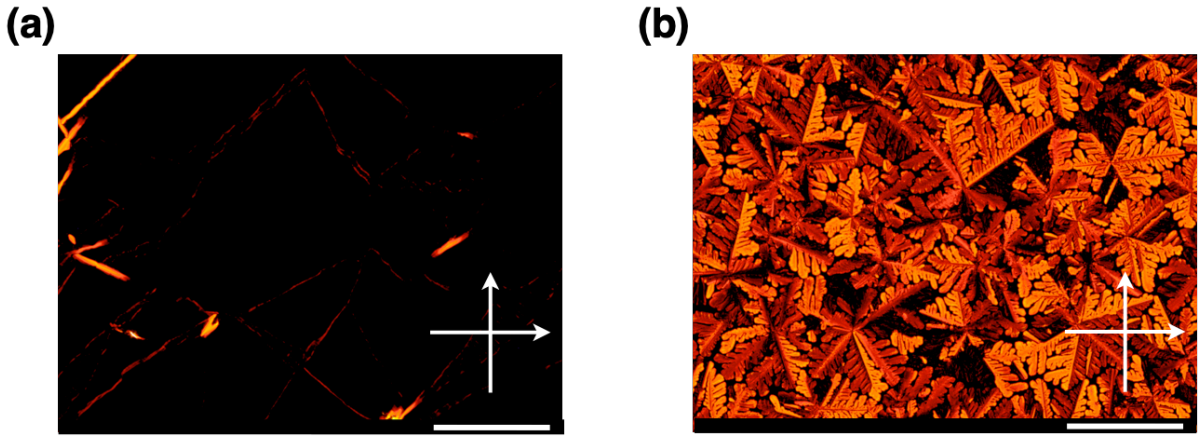

Figure S7. Crossed polarized micrographs at 20 ºC of (a) $\mathbf{1}_{Ni}$ and (b) $\mathbf{1}_{Zn}$ sandwiched between two quartz plates used for TRMC measurements. The samples were cooled at 1 ºC min^{-1} from isotropic phase. The scale bars indicate 100 μm. The bright lines and area in (a) indicate the domain boundaries where parallel orientation of columns takes place.

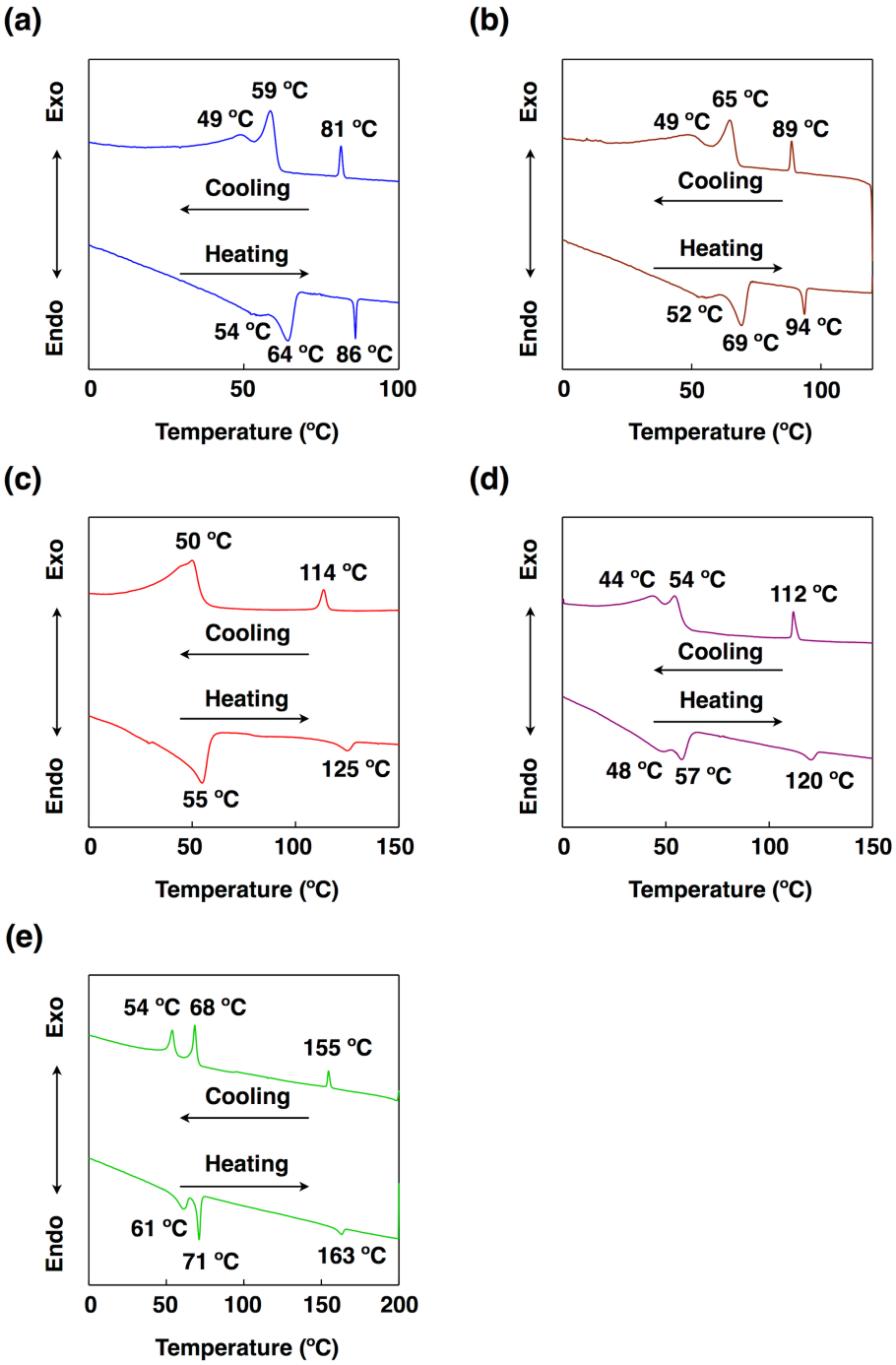

Figure S8. DSC traces with phase transition temperatures of (a) $\mathbf{1}_{\mathbf{Ni}}$, (b) $\mathbf{1}_{\mathbf{2H}}$, (c) $\mathbf{1}_{\mathbf{Cu}}$, (d) $\mathbf{1}_{\mathbf{Pd}}$, and (e) $\mathbf{1}_{\mathbf{Zn}}$ on second heating/cooling at 5 °C min^{-1}.

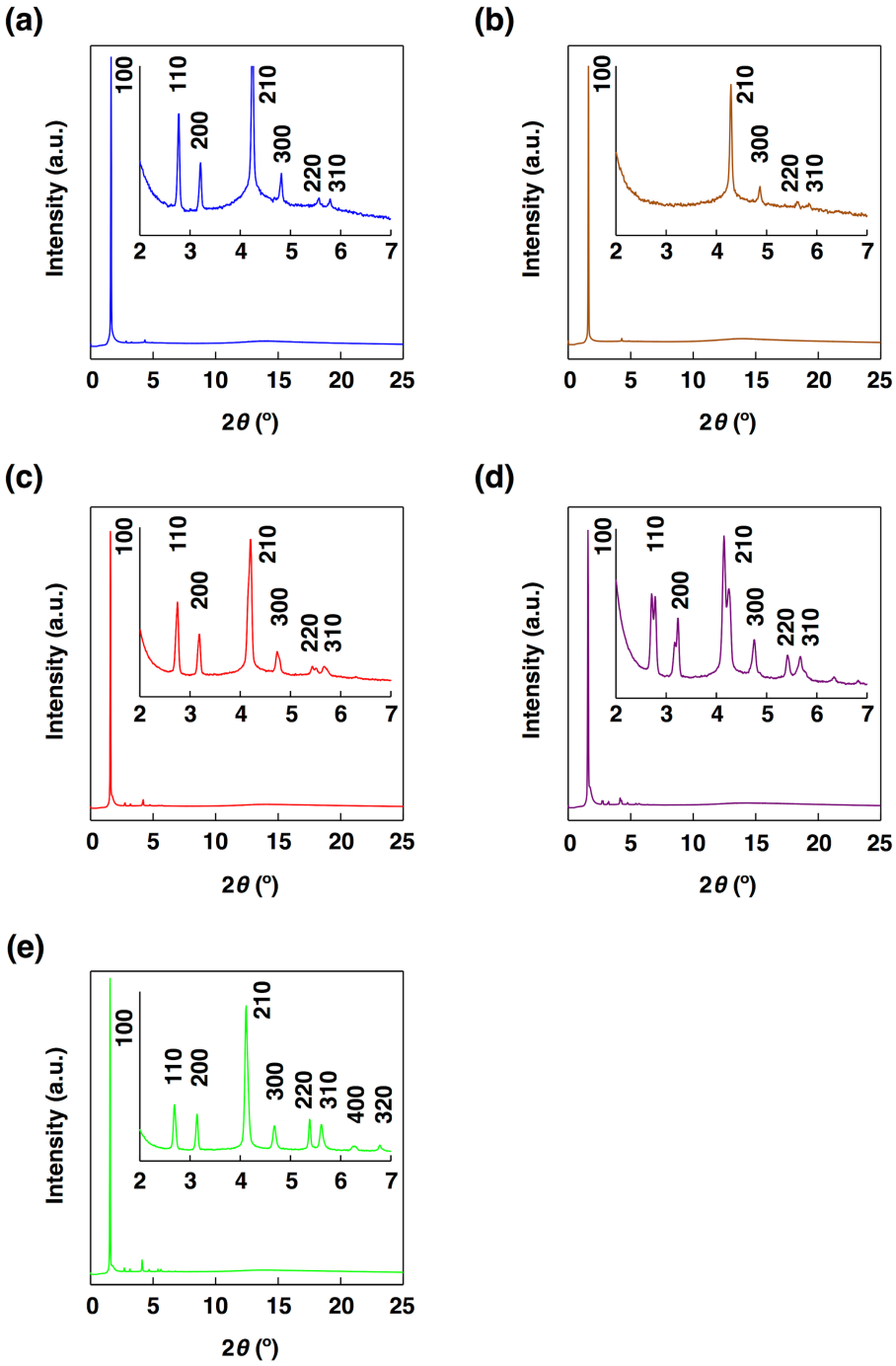

Figure S9. X-ray diffraction patterns of (a) $\mathbf{1}_{Ni}$ at 70 ºC, (b) $\mathbf{1}_{2H}$ at 80 ºC, (c) $\mathbf{1}_{Cu}$ at 90 ºC, (d) $\mathbf{1}_{Pd}$ at 110 ºC, and (e) $\mathbf{1}_{Zn}$ at 150 ºC. The more intense and sharp peaks of (220) and (310) for $\mathbf{1}_{Pd}$ and $\mathbf{1}_{Zn}$ suggest their stronger periodic intermolecular interactions among $\mathbf{1}_{Pd}$ and $\mathbf{1}_{Zn}$ molecules in a local scale.

Table S1. Comparison of calculated and observed spacing values from XRD measurement of (a) $\mathbf{1_{Ni}}$ at 70 ºC, (b) $\mathbf{1_{2H}}$ at 80 ºC, (c) $\mathbf{1_{Cu}}$ at 90 ºC, (d) $\mathbf{1_{Pd}}$ at 110 ºC, and (e) $\mathbf{1_{Zn}}$ at 150 ºC.

(a)

d_{obs} (Å)	d_{cal} (Å)	*hkl*	*hkl*
38.68	38.58	100	020, 110
22.26	22.27	110	200, 130
19.28	19.29	200	220, 040
14.56	14.58	210	310, 240
12.84	12.86	300	330, 060
11.11	11.14	220	400, 260
10.69	10.70	310	420, 350
		a = 44.6 Å	*a* = 44.6 Å
			b = 77.2 Å
		hexagonal	*rectangular*

(b)

d_{obs} (Å)	d_{cal} (Å)	*hkl*	*hkl*
38.20	38.20	100	020, 110
14.43	14.44	210	310, 240
12.71	12.73	300	330, 060
11.00	11.03	220	400, 260
10.60	10.59	310	420, 350
		a = 44.1 Å	*a* = 44.1 Å
			b = 76.4 Å
		hexagonal	*rectangular*

(c)

d_{obs} (Å)	d_{cal} (Å)	*hkl*	*hkl*
39.17	39.05	100	020, 110
22.50	22.55	110	200, 130
19.46	19.53	200	220, 040
14.70	14.76	210	310, 240
13.06	13.02	300	330, 060
11.23	11.27	220	400, 260
10.92	10.83	310	420, 350
		a = 45.1 Å	*a* = 45.1 Å
			b = 78.1 Å
		hexagonal	*rectangular*

(d)

d_{obs} (Å)	d_{cal} (Å)	*hkl*	d_{cal} (Å)	*hkl*
39.17	39.02	100	39.30	110
			38.70	020
22.84	22.53	110	22.81	200
22.26			22.46	130
19.52	19.51	200	19.65	220
19.16			19.35	040
14.91	14.75	210	14.92	310
14.56			14.76	240
13.03	13.01	300	13.10	330
11.42	11.26	220	11.40	400
10.96	10.82	310	10.94	420
	a = 45.1 Å		*a* = 45.6 Å	
			b = 77.4 Å	
	hexagonal		*rectangular*	

(e)

d_{obs} (Å)	d_{cal} (Å)	*hkl*	*hkl*
39.67	39.65	100	020, 110
23.01	22.89	110	200, 130
19.71	19.83	200	220, 040
15.02	14.98	210	310, 240
13.23	13.22	300	330, 060
11.51	11.45	220	400, 260
11.01	11.00	310	420, 350
9.86	9.91	400	440, 080
9.13	9.10	320	420, 350
		a = 45.8 Å	*a* = 45.8 Å
			b = 79.3 Å
		hexagonal	*rectangular*

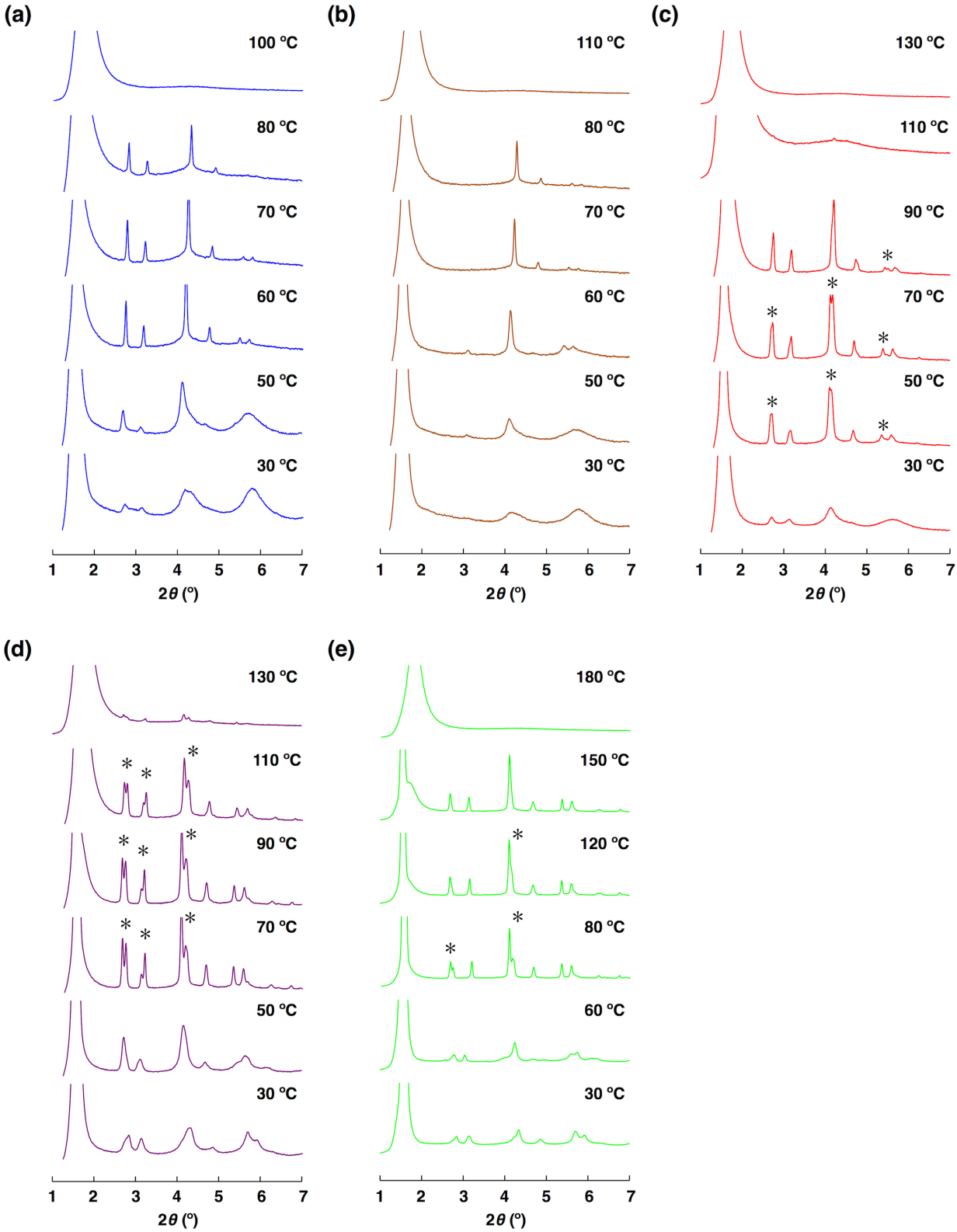

Figure S10. Variable-temperature X-ray diffraction patterns of (a) $\mathbf{1}_{Ni}$, (b) $\mathbf{1}_{2H}$, (c) $\mathbf{1}_{Cu}$, (d) $\mathbf{1}_{Pd}$ and (e) $\mathbf{1}_{Zn}$ upon cooling from isotropic melt. Asterisks indicate a splitting of the peaks that are assignable to a rectangular lattice.

Additional Note:

All the observed peaks can be assigned as (*hk*0) type indexes including the wider angle region, that the $\mathbf{1_M}$ series do not have plasticity (*S8*).

Table S2. Comparison of hexagonal lattice parameter *a* as a function of temperature. *a* was calculated from (100) peaks in XRD.

$\mathbf{1_{Ni}}$	Temp. / ºC	d_{100} / Å	*a* / Å	Phase
	80	37.7	43.5	Col
	70	38.7	44.7	Col
	60	39.2	45.3	Col
	50	39.9	46.1	G (col)
	40	39.9	46.1	G (col)
	30	39.7	45.8	G (col)

$\mathbf{1_{2H}}$	Temp. / ºC	d_{100} / Å	*a* / Å	Phase
	80	38.2	44.1	Col
	70	38.7	44.7	Col
	60	39.4	45.5	G (col)
	50	40	46.2	G (col)
	30	39.9	46.1	G (col)

$\mathbf{1_{Cu}}$	Temp. / ºC	d_{100} / Å	*a* / Å	Phase
	90	39	45.0	Col
	70	39.5	45.6	Col
	50	39.7	45.8	G (col)
	30	39.7	45.8	G (col)

$\mathbf{1_{Pd}}$	Temp. / ºC	d_{100} / Å	*a* / Å	Phase
	110	39.05	45.1	Col
	90	39.4	45.5	Col
	70	39.8	46.0	Col
	50	39.7	45.8	G (col)
	30	39.7	45.8	G (col)

$\mathbf{1_{Zn}}$	Temp. / ºC	d_{100} / Å	*a* / Å	Phase
	150	39.75	45.9	Col
	120	39.67	45.8	Col
	100	39.82	46.0	Col
	80	39.72	45.9	Col
	60	–[a]	–[a]	G (col)
	30	–[a]	–[a]	G (col)

[a] The observed peaks are split into two peaks and too broad, which makes it difficult to analyze the lattice parameter as a hexagonal columnar phase.

Additional Note:

The observed positive correlation between lattice parameter *a* and temperature implies that the stretching of the alkyl chains with decreasing temperature results in an increase in the lattice parameter (*S9*). Upon lowing the temperature from the columnar mesophase, the decrease of *a* was observed (see 30 ºC in $\mathbf{1_{Ni}}$, 30 ºC in $\mathbf{1_{2H}}$, and 50 and 30 ºC in $\mathbf{1_{Pd}}$), which suggests the interdigitation of alkyl chains of the molecules.

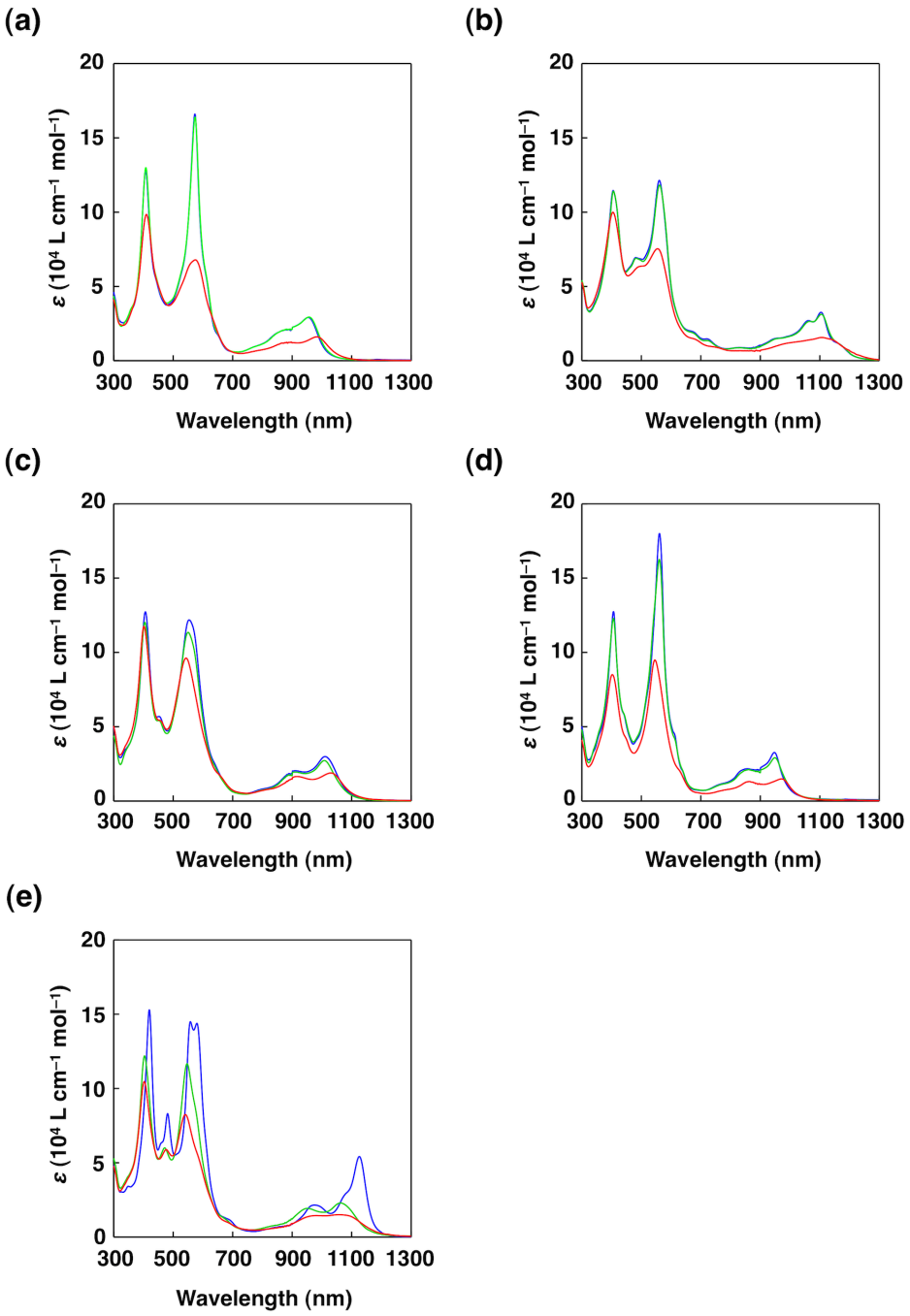

Figure S11. Absorption spectra of (a) $\mathbf{1}_{\mathbf{Ni}}$, (b) $\mathbf{1}_{\mathbf{2H}}$, (c) $\mathbf{1}_{\mathbf{Cu}}$, (d) $\mathbf{1}_{\mathbf{Pd}}$, and (e) $\mathbf{1}_{\mathbf{Zn}}$ at 25 ºC in THF (blue), CH_2Cl_2 (green), and cyclohexane (red).

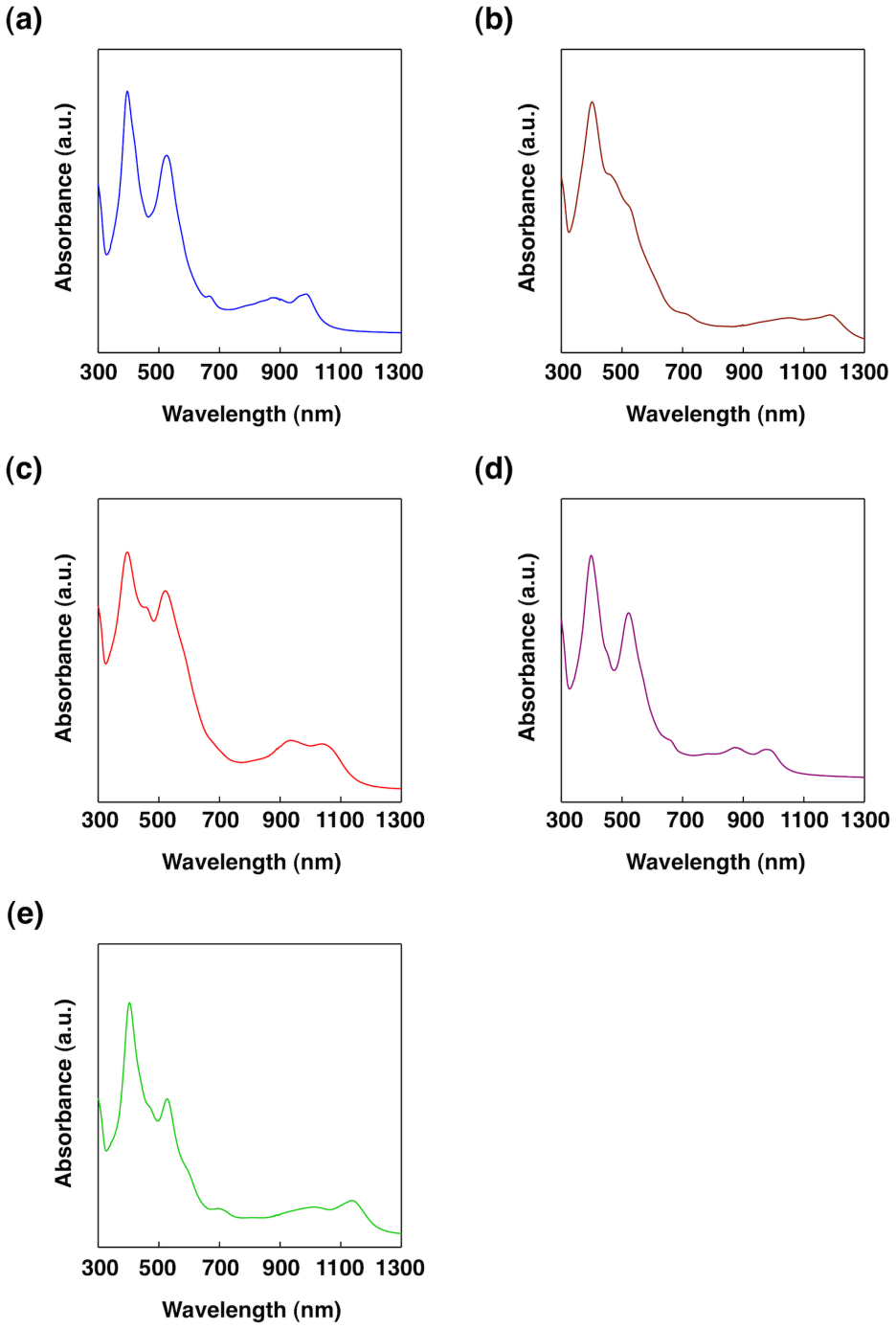

Figure S12. Absorption spectra of films at 25 ºC of (a) $\mathbf{1}_{\mathbf{Ni}}$, (b) $\mathbf{1}_{\mathbf{2H}}$, (c) $\mathbf{1}_{\mathbf{Cu}}$, (d) $\mathbf{1}_{\mathbf{Pd}}$, and (e) $\mathbf{1}_{\mathbf{Zn}}$.

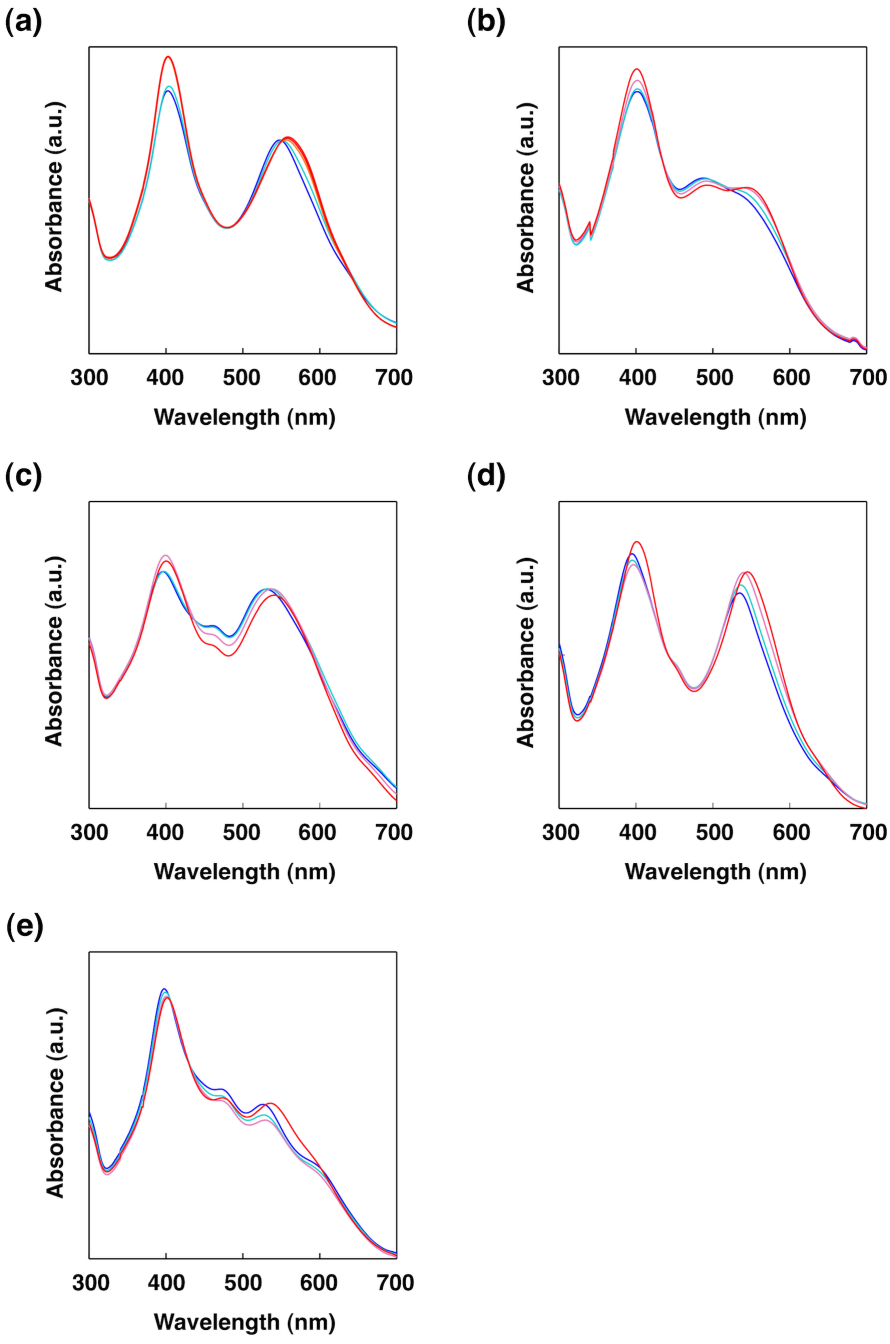

Figure S13. Variable-temperature absorption spectra of films of (a) $\mathbf{1}_{\mathbf{Ni}}$ on heating from 80 (blue) to 100 (red) ºC, (b) $\mathbf{1}_{\mathbf{2H}}$ on heating from 70 (blue) to 110 (red) ºC, (c) $\mathbf{1}_{\mathbf{Cu}}$ on heating from 80 (blue) to 140 (red) ºC, (d) $\mathbf{1}_{\mathbf{Pd}}$ on heating from 80 (blue) to 140 (red) ºC, and (e) $\mathbf{1}_{\mathbf{Zn}}$ on heating from 80 (blue) to 170 (red) ºC.

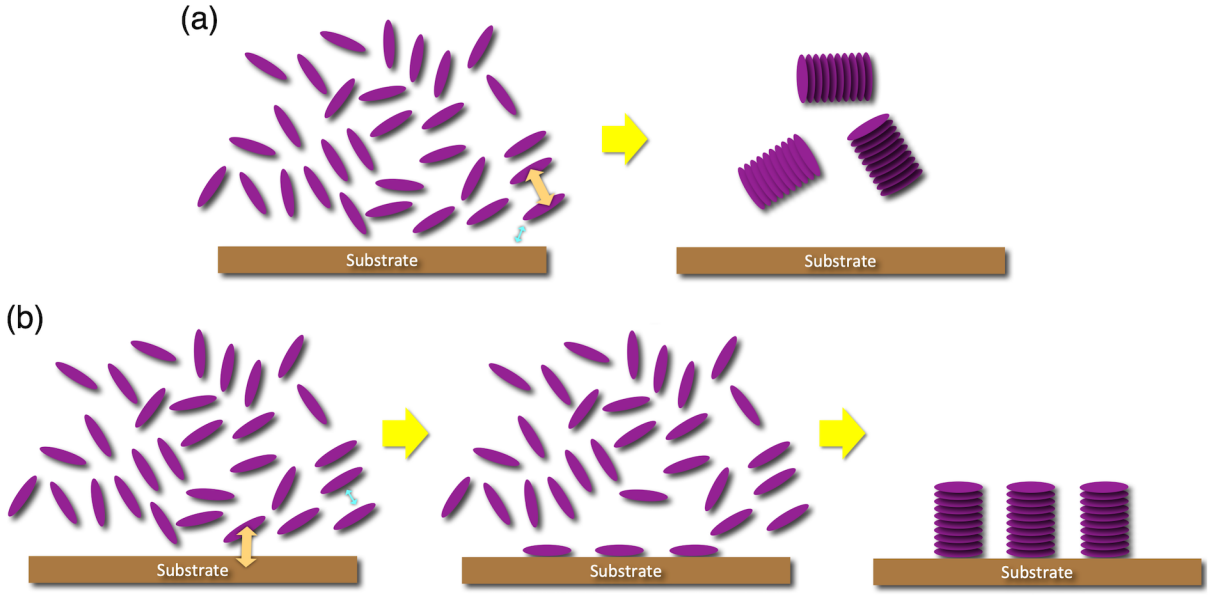

Figure S14. Schematic illustration of possible mechanism of random or homeotropic alignment of columns for discotic LC molecules with relatively (a) strong and (b) weak π-π (core-to-core) interactions. π-π interactions with isotropic directions happen in (a), while nucleation at the substrate–material interface takes place followed by the growth of columns in (b).

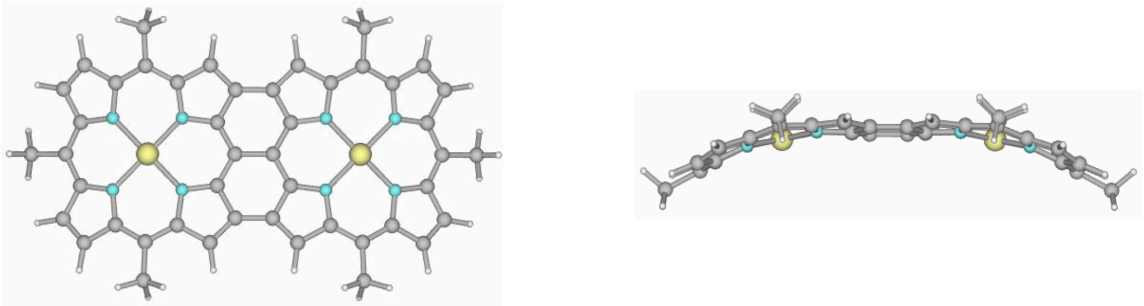

Figure S15. Top and side views of two types of optimized ground-state structures of the Ni complex of the *meso*-methyl fused porphyrin dimer at the level of B3LYP/6-31G(d) (TZVP for Ni).

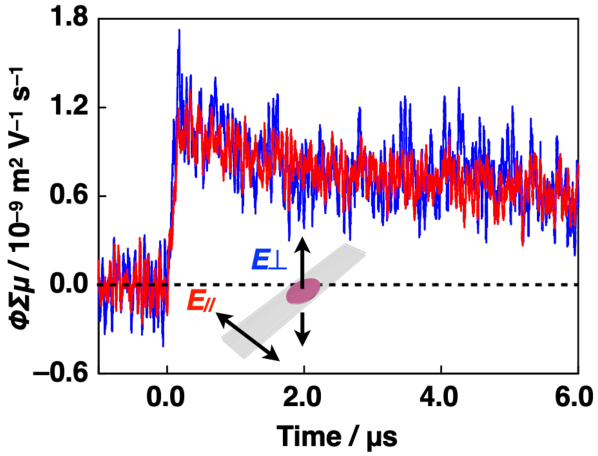

Figure S16. (a) Photoconductivity transients of $\mathbf{1_{Zn}}$ at 20 °C upon photoexcitation at 355 nm. The red and blue plots are the conductivity along the electric field directions parallel ($E_{//}$) and perpendicular ($E_{\perp}$) to the substrate plane, respectively.

4. Supporting References

(S1) A. D. Becke, *Phys. Rev.,* 1988, **A38**, 3098–3100.

(S2) A. D. Becke, *J. Chem. Phys.,* 1993, **98**, 1372–1377.

(S3) C. Lee, W. Yang, R. G. Parr, *Phys. Rev.,* 1988, **B37**, 785–788.

(S4) M. J. Frisch, *et al., Gaussian 09*, Revision B.01, Gaussian, Inc., Wallingford, CT **2010**.

(S5) F. Tanaka, K. Kinoshita, R. Tanimura, I. Fujii, *J. Am. Chem. Soc.,* 1996, **118**, 2332–2339.

(S6) V. Percec, *et al.*, *Chem. Eur. J.* 2009, **15**, 8994–9004.

(S7) J. Otera, N. Dan-oh, H. Nozaki, *J. Org. Chem.,* 1991, **56**, 5307–5311.

(S8) B. Glüsen, A. Kettner, J. H. Wendorff, *Mol. Cryst. Liq. Cryst.*, 2006, **303**, 115–120.

(S9) S. K. Prasad, D. S. Shankar Rao, S. Chandrasekhar, S. Kumar, *Mol. Cryst. Liq. Cryst.*, 2003, **396**, 121–139.